

# Estimation of geostrophic current in the Red Sea based on Sea level anomalies derived from extended satellite altimetry data

Ahmed M Taqi<sup>a,b</sup>, Abdullah M Al-Subhi<sup>a</sup>, Mohammed A Alsaafani<sup>a</sup> and Cheriye P  
Abdulla<sup>a</sup>

<sup>a</sup>Department of Marine Physics, King Abdulaziz University, Jeddah, Saudi Arabia;

<sup>b</sup>Department of Marine Physics, Hodeihah University, Hodeihah, Yemen

Correspondence to: Ahmed. M. Taqi (ataqi@stu.kau.edu.sa)

## Abstract

The geostrophic currents near the coast of the Red Sea has a large gap. Due to **this**, the sea level anomaly (SLA) data of Jason-2 has been reprocessed and extended towards the coast of the Red Sea and merged with AVISO data at the **offshore region**. The processing has been applied to build a data grid to achieve best results for the SLA and geostrophic current. The results obtained from the new extended data at the coast are more consistent with the observed data (CTD) and hence geostrophic current calculation. The pattern of SLA distribution and geostrophic currents are divided into two seasons; winter season extends from October to May and summer from June to September. The geostrophic currents along the eastern Red Sea flow toward north and southward along the west coast. This flow is modified with the presence of the cyclonic and anticyclonic eddies, which are more concentrated in the central and northern Red Sea. **The results show anticyclonic eddies (AE) on the eastern side of the Red Sea and cyclonic eddies (CE) on the western side during winter. During summer, the (CE) are along the eastern side and (AE) along the western side. In summer, cyclonic eddies are more dominant for the entire Red Sea while in winter both cyclonic and anticyclonic eddies are present. Furthermore, the lifespan of cyclonic eddies are longer than that of anticyclonic eddies. This study is the first of this type in the Red Sea which extend SLA and geostrophic**

currents to the coastal region and provide the closed contour structure of the eddy in the coastal region.

## 1. Introduction

The Red Sea is a narrow semi-enclosed water body that lies between continents of Asia and Africa. It is located between latitude 12.5°-30°N and longitude 32°E-44°E in an NW-SE orientation. Its average width is 220 km and the average depth is 524 m (Patzert, 1974). It is connected at its northern end with the Mediterranean Sea through the Suez Canal and at its southern end with the Indian Ocean through the strait of Bab El- Mandab. The exchange of water through Bab El- Mandab (shallow sill of 137 m) is the most significant factor that determines the oceanographic properties of the Red Sea (Smeed, 2004).

During winter, the southern part of the Red Sea is subject to SE monsoon wind, which is relatively strong from October to December, with a speed of 6.7-9.3 ms<sup>-1</sup> (Patzert, 1974). During the summer season, the wind is shifting its direction to be from NW. On the other hand, in the northern part of the Red Sea, the dominant wind is NW all year around.

The circulation in the Red Sea is driven by strong thermohaline and wind forces (Neumann and McGill, 1961; Phillips, 1966; Quadfasel and Baudner, 1993; Siedler, 1969; Tragou and Garrett, 1997). Several studies in the Red Sea have focused on thermohaline circulation, where they found that the exchange flow between the Red Sea and Gulf of Aden consists of two layers in winter and three layers in summer through Bab El- Mandab (e.g. Phillips 1966; Tragou and Garrett 1997; Murray and Johns 1997; S. Sofianos and Johns 2015; Al Saafani and Shenoi, 2004; Smeed, 2004). Other studies describe the basin-scale circulation based on modelling approach, usually forced at a relatively low-resolution (1°) by buoyancy flux and global wind (Clifford et al., 1997; Sofianos, 2003; Tragou and Garrett, 1997; Biton et al., 2008; Yao et al., 2014a,b). The horizontal circulation in the Red Sea consists of several eddies, some of them are semi-permanent eddies (Quadfasel and Baudner, 1993), that often present during the winter (Clifford et al., 1997; Sofianos and Johns, 2007) in the northern Red Sea. The circulation system in the central Red Sea is dominated by cyclonic (CE) and anticyclonic eddies (AE), mostly between 18°N and 24°N. Eddies are also found in the southern Red Sea but not in a continuous pattern (Johns et al., 1999). Zhan et al., (2014) reported recurring or persistent eddies in the north and the central Red Sea,

although there are differences in the number of eddies, their location, and type of vorticity (cyclonic or anticyclonic).

The long-term sea level variability in the Red Sea is largely affected by the wind stress and the combined impact of evaporation and water exchange across the strait of Bab El Mandeb (Edwards, 1987; Sultan et al., 1996). The Sea level in the Red Sea is higher during winter and lower during summer (Edwards, 1987; Sofianos and Johns, 2001; Manasrah et al., 2004). It is characterized by two cycles, annual and semi-annual, where the annual cycle is dominant (Abdallah and Eid, 1989; Sultan and Elghribi, 2003).

In recent years, there has been an increasing interest for using satellite altimetry Sea level anomaly (SLA) which offer large coverage and long data period for providing measurements of SSH, wave height and wind speed (Chelton et al., 2001). However, the altimeter data undergoes several processing stages for corrections due to the atmosphere and ocean effects (Chelton et al., 2001). The satellite altimetric data has been used for the open ocean for a long time with great success, while the data of the coastal region suffers from gaps of almost 50 km from the coastline. The coastal region requires further corrections due to additional difficulties based on the closeness of the land (Deng et al., 2001; Vignudelli et al., 2005; Desportes et al., 2007; Durand et al., 2009; Birol et al., 2010). In the past two decades, many researchers have sought to develop different methods to improve the quality, accuracy and availability of altimetric data near the coast (e.g. Vignudelli et al., 2000; Deng and Featherstone, 2006; Hwang et al., 2006; Guo et al. 2009, 2010; Vignudelli et al., 2005; Desportes et al., 2007; Durand et al., 2009; Birol et al., 2010; Khaki et al., 2014; Ghosh et al., 2015; Taqi et al., 2017). The satellite altimetry faces three types of problems near the coast; (1) the echo interference with the surrounding ground as well as the inland water surface reflection (Andersen and Knudsen, 2000; Mantripp, 1966), (2) environmental and geophysical corrections such as dry tropospheric correction, wave height, high frequency and tidal corrections from global models, etc. and (3) spatial and temporal corrections during sampling (Birol et al., 2010).

The ocean currents circulate water worldwide. They have significant influence on the transfer of energy and moisture between the ocean and the atmosphere. Ocean currents play a significant role in climate change in general. In addition, they contribute to the distribution of hydrological characteristics, nutrients, contaminants and other dissolved materials between the

coastal and the open areas, and among the adjacent coastal regions. Ocean currents carry sediment from and to the coasts, so play a significant role in shaping of the coasts. That is important in the coastal region where in the densely inhabited coastal region, producing large amounts of pollutants. Understanding of the currents helps us in dealing with the pollutants and coastal management.

The objective of the present research is to study the geostrophic current in the Red Sea including the coastal region using the modified along track Jason-2 SLA along the coast produced by Taqi et al., (2017).

## **2. Material and Methods**

### **2.1. Description of data**

#### ***2.1.1 Fourier series model (FSM) SLA***

The SLA data used in this study is weekly Jason-2 along the track from June 2009 (cycle 33) to October 2014 (cycle 232) which has been extended to the coastal region by Taqi et al., (2017) by applying the FSM method. The extended data shows a good agreement with the coastal tide gauge station data. In brief, the FSM method of extending SLA consists of four steps; the first step is the removal from SLA the outliers which are outside three times standard deviation from mean. Second step; the SLA is recomputed using Fourier series equation along the track. Third step; the data is then filtered to remove the outliers in the SLA with time similar to the first step. Finally, the SLA data is linearly interpolated over the time to form the new extended data which is called FSM. For more details on the FSM method, refer to Taqi et al., (2017).

#### ***2.1.2 AVISO, Tide Gauge, and hydrographic datasets***

This study uses two types of SLA data; The first set is the (SLA), which has been downloaded from the Archiving Validation and Interpretation of Satellite Oceanographic (AVISO) (<ftp://ftp.aviso.altimetry.fr/global/delayed-time/grids/msla/all-sat-merged>). The second dataset is the SLA from the extended FSM data. The temperature and salinity profiles used for geostrophic estimation are received from three cruises, the first cruise was during March 16 to 29, 2010 onboard R/V Aegaeo with a total of 111 Conductivity, Temperature and Depth (CTD) profiles. For more details; see Bower and Farrar (2015). The second cruise was on April 3 to 7, 2011 onboard Poseidon and the third one was during October 16 to 19, 2011 as a part of Jeddah transect, KAU-KEIL Project. For more details; consult R/V POSEIDON cruise P408/1 report (Schmidt et

al., 2011). Finally, three tide gauges data at the eastern coastline of the Red Sea are obtained from the General Commission of Survey (SGS) at the Kingdom of Saudi Arabia (Fig.1) and their location details are shown in Table 1.

## 2.2 Method

The SLA data used in this study are coming from two sources: (1) the FSM data near the coast and (2) the AVISO data along the axis of the Red Sea. The steps to merge the two datasets and calculating the geostrophic currents are given below.

First, the along-track FSM data are used to produce gridded data to a spatial resolution of  $0.25^\circ \times 0.25^\circ$  for the comparison with Aviso data. The second step, the coastal FSM gridded data then combined with AVISO offshore data, to produce combined  $0.25^\circ \times 0.25^\circ$  SLA data extended toward the coast (here and after will be called FSM-SLA). Finally, surface geostrophic currents are estimated from FSM-SLA data using the following equation;

$$u_g = -\frac{g}{f} \frac{\partial \zeta}{\partial y} \quad v_g = \frac{g}{f} \frac{\partial \zeta}{\partial x} \quad (2)$$

Where  $(u_g, v_g)$  is the surface geostrophic current,  $g$  is gravity,  $f$  is the Coriolis parameter and  $\zeta$  is the sea surface height. The estimation of geostrophic currents from CTD data is using the following equation;

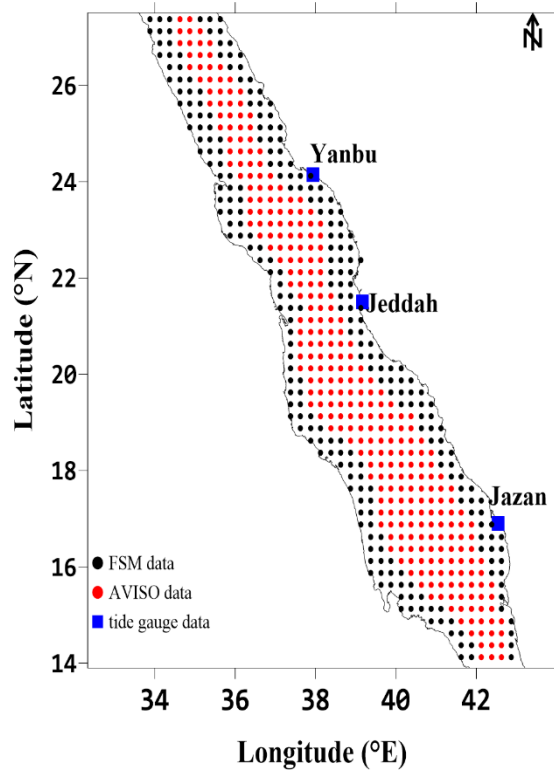
$$u_g = -\frac{1}{f\rho} \frac{\partial p}{\partial y} \quad v_g = \frac{1}{f\rho} \frac{\partial p}{\partial x} \quad (2)$$

where  $\rho$  is the density of seawater,  $p$  is hydrostatic pressure derived from the density. The stations have depths that vary from 50 up to 2344 m. However, most of the stations (~90 %) exceed the 500 m depth, accordingly the level of on motion set to 500m.

Table 1. The location of tide gauge stations and period of measurement.

Station	Latitude	Longitude	Period
Jazan	16.87	42.55	1/9/2012 to 31/8/2013
Jeddah	21.42	39.15	1/9/2012 to 31/8/2013
Yanbu	23.95	38.25	1/9/2012 to 31/8/2013

140



141 Figure 1. show the study area and the grid-points locations with a spatial resolution of  $0.25^\circ \times$   
142  $0.25^\circ$  and locations of the tide gauges.

### 143 3. Result and Discussion

#### 144 3.1 Validation of FSM-SLA and geostrophic current

145 The statistical analysis has been conducted to show the quality of FSM-SLA as compared  
146 with AVISO. The Correlation Coefficient (CC) reveals a good agreement between the two datasets  
147 in the open sea (about 0.7 to 0.9) and is shown in Fig. 2. Near the coasts, on the other hands, shows  
148 weak correlation coefficient between the two data sets; 0.45 to 0.7.

149 Furthermore, the observed SLA from the coastal tide gauge is compared with the FSM-  
150 SLA data and AVISO datasets. Table 2. illustrates some of the statistical analysis, where the root  
151 mean square error (RMSE) is lower for FSM-SLA as compared to that of AVISO.

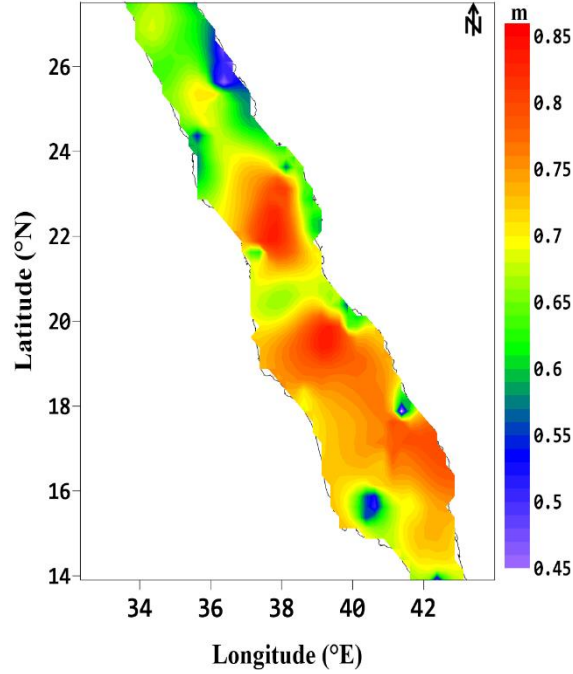


Figure 2. show the correlation coefficient between AVISO and FSM data

Table 2. statistical analysis for AVISO and FSM-SLA data with observed data ( in 2013).

	Jasan		Jeddah		Yanbu	
	FSM-SLA	AVISO	FSM-SLA	AVISO	FSM-SLA	AVISO
CC	0.936	0.914	0.915	0.906	0.907	0.895
RMSE(m)	0.073	0.085	0.069	0.094	0.067	0.104
Note: The p-value corresponding to all comparison is very low ( $P < 0.0001$ ), indicating that the results from correlation are significant.						

Figure 3 shows the SLA time series for 2013 from the three coastal stations as compared with the FSM-SLA and AVISO. The three stations datasets have similar seasonal pattern and FSM-SLA coincides with observed SLA in shorter-duration fluctuations. This agreement is clearly shown in Table 2. The comparison of FSM-SLA data and the observed SLA data (at Jazan, Jeddah, and Yanbu stations) show a better correlation than between the AVISO and observed SLA data as shown in Fig.3 and Table .2. These correlation coefficient differences indicate that the FSM-SLA

shows better accuracy near the coast. These results were consistent with those obtained for along-track Jason-2 SLA with coastal stations by Taqi et al., (2017).

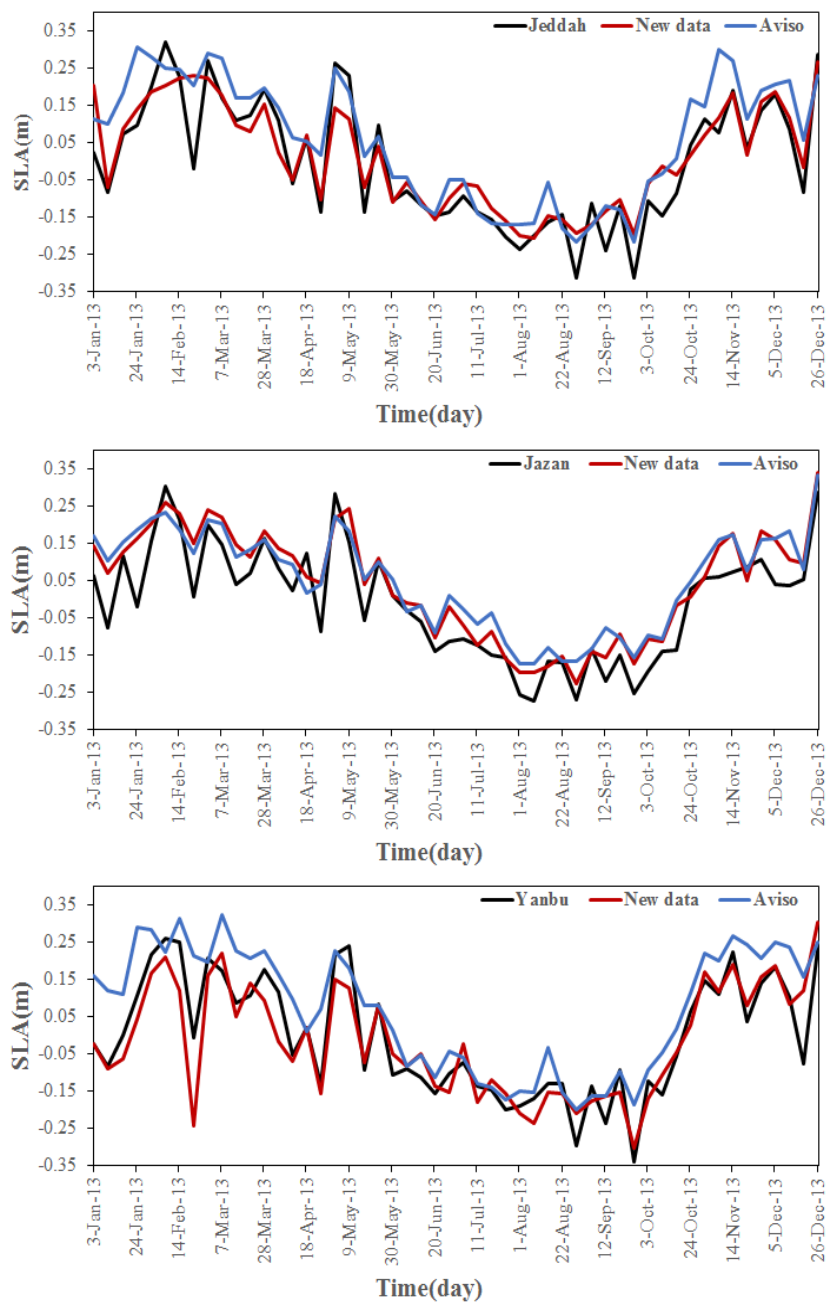


Figure 3. Comparison of SLA from three tide gauge (black), with grid FSM-SLA data (red) and Aviso (blue)



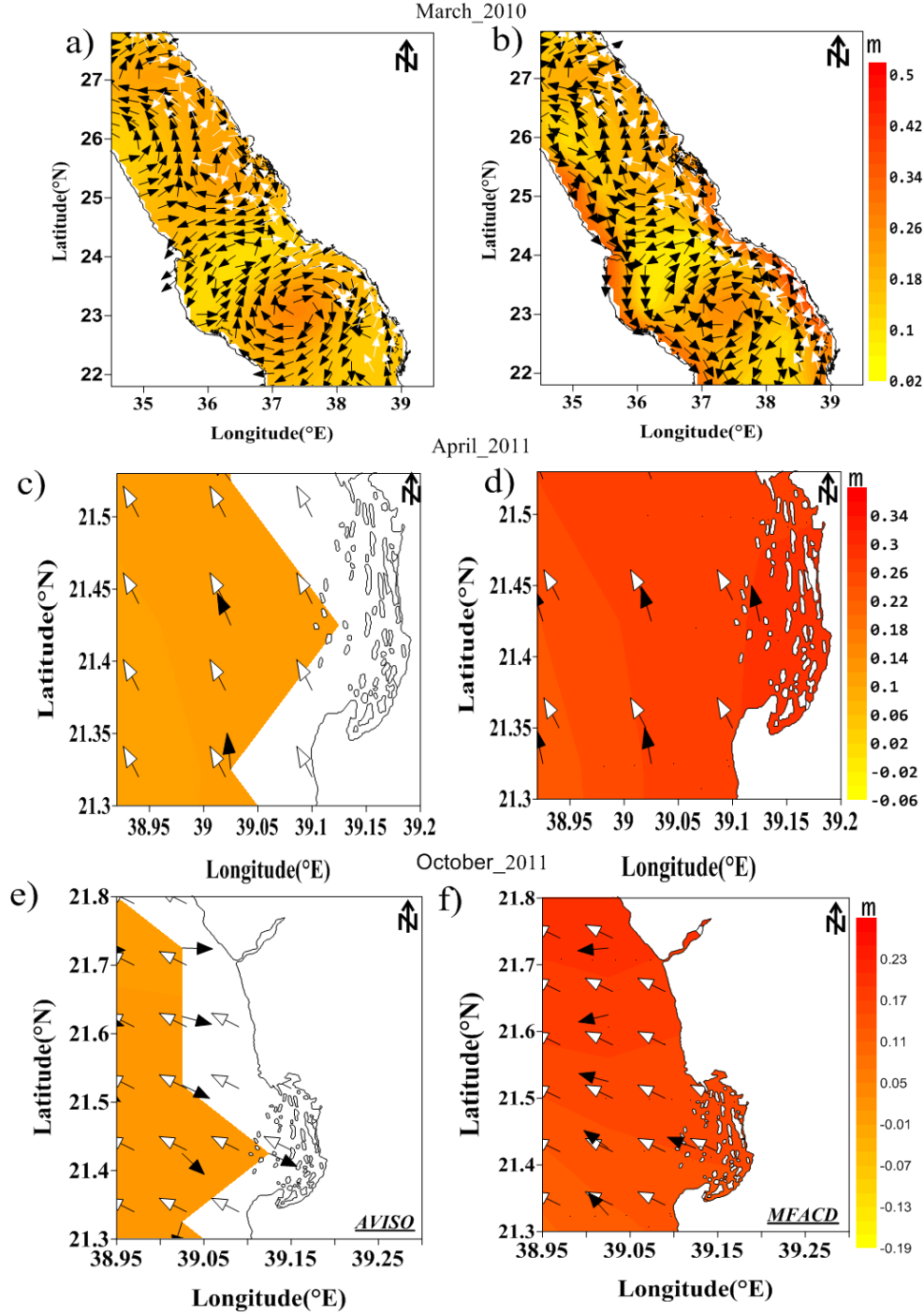


Figure 4. Comparison for three months' SLA (color) and geostrophic currents (black vectors) between (left) AVISO and (right) FSM-SLA white vectors show geostrophic currents from CTD data.

Figure 4 shows a comparison between the geostrophic currents for the central Red Sea derived from AVISO and FSM-SLA for three different times (March 2010, April 2011, and

October 2011), those different periods corresponding to the timing of three cruises described in section 2.1.

It can be seen from the Fig. 4(b, d & f) that there is a significant matching in the directions of geostrophic currents from FSM-SLA with CTD data near the coast and offshore. This result is in agreement with Bower and Farrar (2015) findings, especially in October 2011 ( Fig. 4f). In March 2010, the geostrophic current near the coast estimated from FSM-SLA is in match with directions of CTD-derived geostrophic current in most regions. However, the directions of geostrophic currents from AVISO are not always in match with CTD-derived one especially in October 2011.

In March 2010 the geostrophic currents along the eastern coast of the Red Sea are towards the north for both FSM-SLA and AVISO, except between 22.2° – 23°N, where the FSM-SLA and CTD data geostrophic currents are in the same direction while AVISO geostrophic current is in the opposite direction (see Fig. 4a,4b).

Table 3. statistical analysis for the speed of geostrophic current from FSM-SLA and AVISO compared with CTD-derived geostrophic current from the thress cruises.

			Bias (m/s)	RMSE (m/s)	Stdv (m/s)	CC
current speed	FSM-SLA	10-Mar	0.13	0.17	0.11	0.54
	AVISO		-0.01	0.07	0.07	0.47
	FSM-SLA	11-Apr	-0.28	0.31	0.15	0.61
	AVISO		-0.87	0.89	0.21	0.44
	FSM-SLA	11-Oct	-0.19	0.49	0.45	0.53
	AVISO		-0.51	0.70	0.48	0.49

The speed of geostrophic current data derived from FSM-SLA and CTD during the months (March 2010, April 2011, October 2011) shows a stronger correlation compared with the speed of geostrophic current derived from AVISO and CTD as shown in Fig. 4 and Table 3.

### 3.2 Description of FSM-SLA and geostrophic current

Figure 5 shows monthly climatology variation for the 6-year period for SLA and geostrophic current. The SLA is higher during the period from October to May and lower during rest of the year, this pattern is consistent with previous studies (Patzert, 1974; Edwards, 1987; Ahmad and Sultan, 1989; Sofianos and Johns, 2001; Sultan and Elghribi, 2003; Manasrah et al., 2004, 2009). Based on calculations made here, the geostrophic current of Red Sea along the eastern coast is northward while along the western coast is southward. This northward flowing current is consistent with a previous study by Bower and Farrar (2015). Similar results are also obtained from three-dimensional modeling by (Clifford et al., 1997; Eshel and Naik, 1997; Sofianos, 2003, 2002). The Fig.5 presents the surface circulation during January in the northern part, where two eddies formed between  $25^{\circ} - 27.5^{\circ}\text{N}$ . The first eddy is an anticyclone between  $26.3^{\circ} - 27.5^{\circ}\text{N}$  on the eastern side of the Red Sea. The other eddy is cyclonic located between  $25^{\circ} - 26.3^{\circ}\text{N}$  near the western coast. To the south of that, there are two other eddies between  $22.5^{\circ} - 24.7^{\circ}\text{N}$ , cyclonic on the western side and anticyclonic on the eastern side. These results match those observed in previous studies by (Eladawy et al., 2017; Sofianos and Johns, 2003a). Two cyclonic eddies and an anticyclonic eddy found at  $19.5^{\circ} - 22.5^{\circ}\text{N}$  are consistent with those modeled by Sofianos and Johns, (2003). Near Bab al-Mandab, there is a cyclonic eddy on the western side between  $15^{\circ} - 16.5^{\circ}\text{N}$ .

In February, the surface circulation of the Red Sea is similar to that during January, with some differences in the eddies structure. The anticyclonic eddy near  $27^{\circ}\text{N}$  on the eastern sides of the Red Sea starts shifting toward the western coast, while a cyclonic eddy at  $25^{\circ} - 26.3^{\circ}\text{N}$  start appearing. The cyclonic eddies between  $22.5^{\circ} - 24.7^{\circ}\text{N}$  on the western side are less clear in this month.

In March and April, all the eddies are located along the central axis of the Red Sea. In the north, the anticyclonic eddy near  $27^{\circ}\text{N}$  is shown in both months, while the cyclonic eddy is not clear during March and April. The anticyclonic eddy shown near  $23-24^{\circ}\text{N}$  during March is weakening during April. **Also, the anticyclonic eddy between  $19-20^{\circ}\text{N}$  is shrinking during April.**

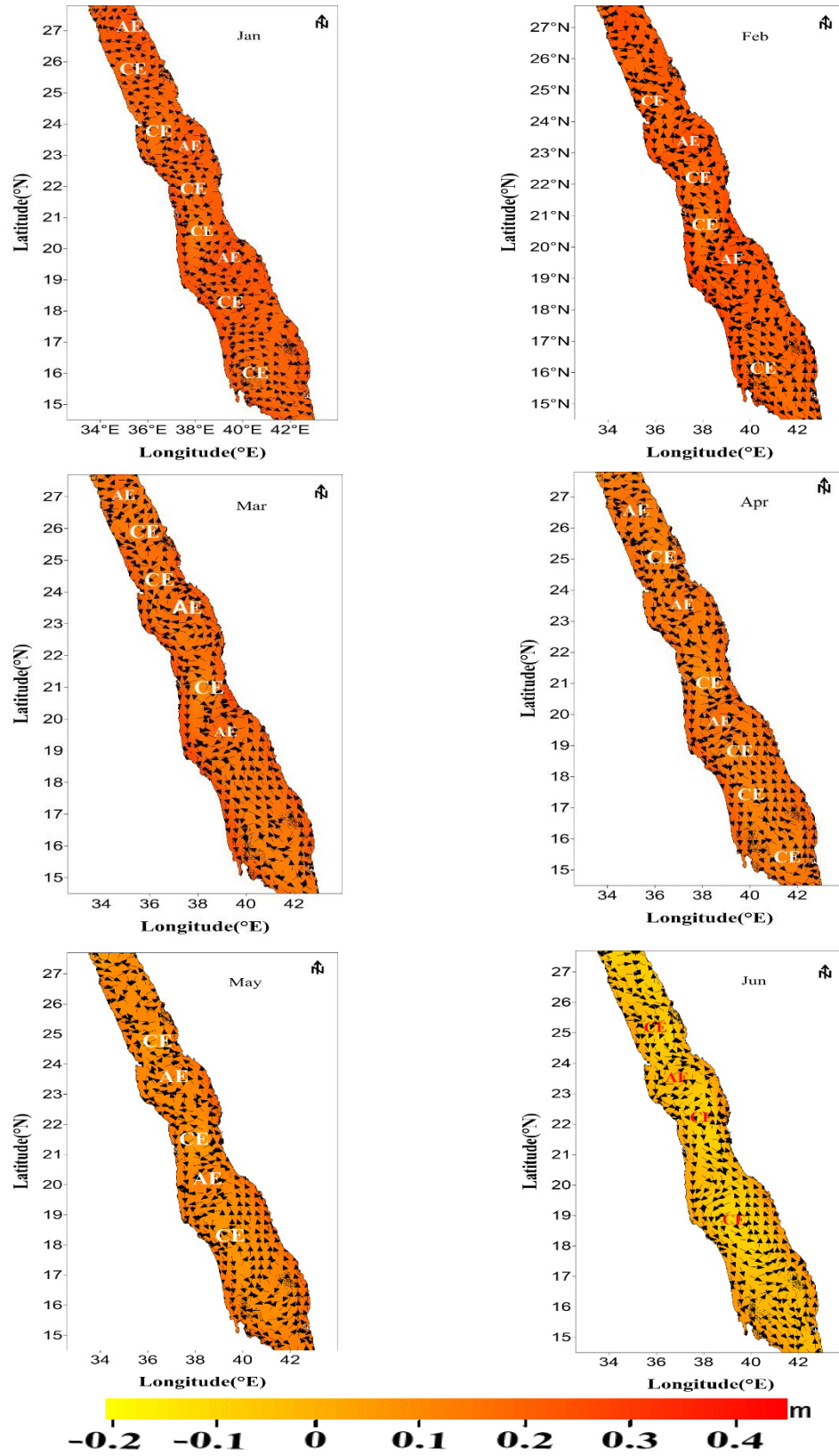
In May, there is no clear eddy between  $27.5^{\circ}\text{N}$  and  $25^{\circ}\text{N}$ . However, four eddies are clearly existing between  $19.5^{\circ} - 25^{\circ}\text{N}$ ; two cyclonic eddies at  $24^{\circ} - 25^{\circ}\text{N}$ , and  $20^{\circ} - 22^{\circ}\text{N}$ , two anticyclonic eddies at  $23^{\circ} - 24^{\circ}\text{N}$ , and  $19.5^{\circ} - 20^{\circ}\text{N}$ . From the previous results, it can be seen several cyclonic

and anticyclonic eddies distributed all over the Red Sea and these results match those in modelling studies (Clifford et al., 1997; Eladawy et al., 2017; Sofianos, 2003, 2002, Yao et al., 2014a)

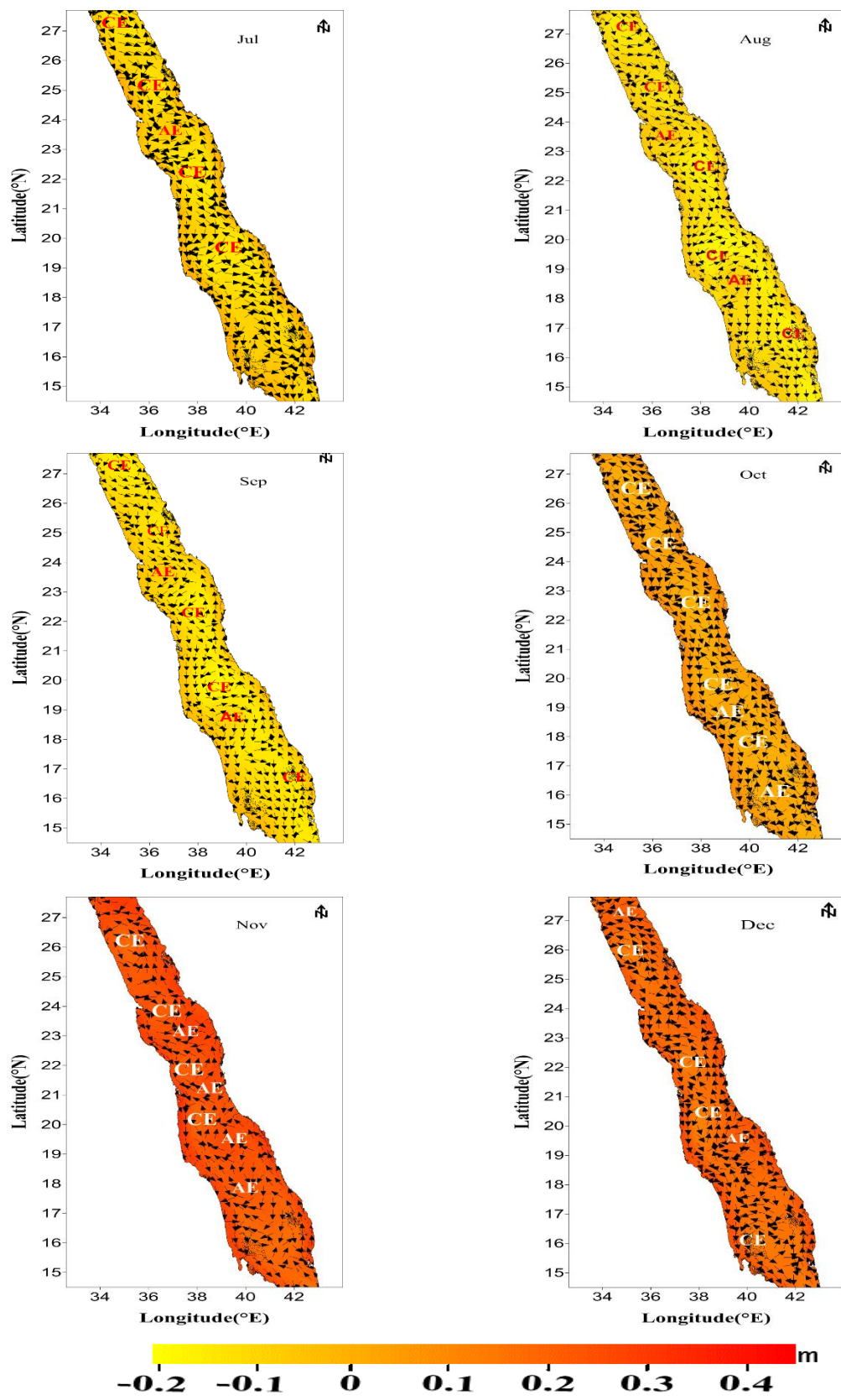
During June, the flow of the geostrophic currents in the northern part reversed its direction. This accompanies a formation of large cyclonic eddy extending from 25.5°– 27.5°N occupying the entire width of the Red Sea. To the south of it, another cyclonic eddy observed between 24°– 25°N and an anticyclonic eddy between 23° – 24°N are also noticed during June with a similar strength during May. The cyclonic eddy seen between 17° – 20°N during May, is also seen during this month with more strength. To the south of it, the flow is towards the Bab el-Mandab following normal summer pattern. The flow pattern along the coast is similar to results of (Chen et al., 2014) for winter (January to April). The short-term climatology of geostrophic current in the Red Sea is dominated by cyclonic and anticyclonic eddies all over the Red Sea, and especially in the central and northern parts of the sea.

During July-September, the flow of the geostrophic currents structure is similar to that of June with two cyclonic eddies north of 24.5°N and an anticyclonic eddy between 23°– 24°N. South of these eddies, another cyclonic eddy extends to 19°N. Furthermore, south of 19°N, there is an outflow towards the south all over the width of the Red Sea with narrow inflow along the eastern coast of the Red Sea. The Fig. 6 also shows an anticyclonic between 18°-19°N and a cyclonic between 16°-17°N during August and September. These results are consistent with the results from previous studies (Clifford et al., 1997; Eladawy et al., 2017; Sofianos, 2003, 2002, Yao et al., 2014b).

During summer (June-September), the changes in wind speed and direction cause reversed of changes in the direction of flow consequently, the locations of eddies are also changed (Chen et al., 2014). The surface current flows from the Red Sea to the Gulf of Aden through the Bab-el-Mandeb. The anticyclonic eddy shown in the north at 27.5°N in winter is replaced with cyclonic eddy, during this season. Summer is dominated by cyclonic eddies as shown in Fig. 6.



251 Figure 5. shown monthly climatology for geostrophic current and Sea level anomaly (Reference  
 252 current length =0.5m/s)



253 Figure 6. As Fig. 5 for July to December

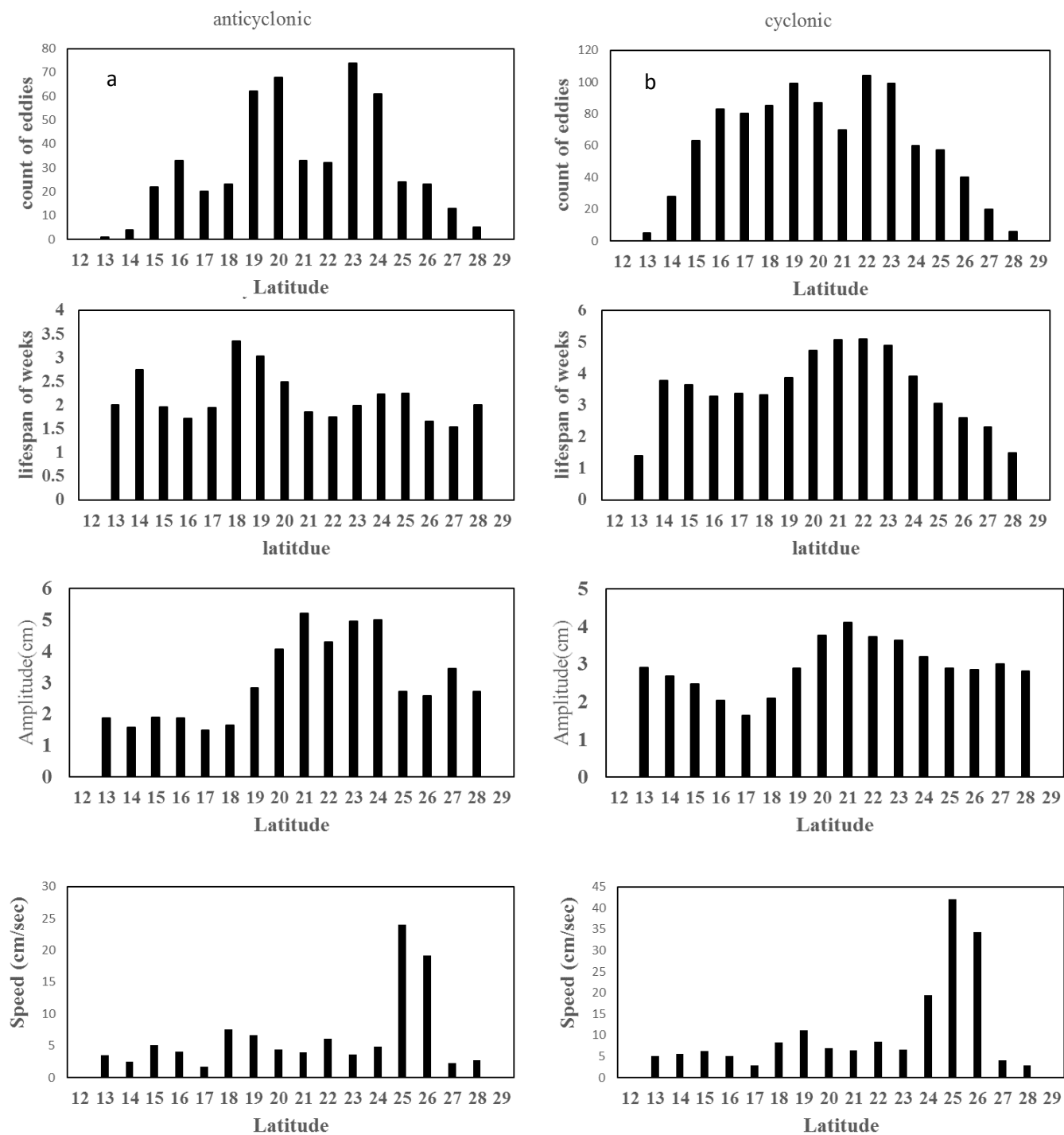
During October, the geostrophic current is weak as compared with that during September, still cyclonic but with less strength. The anticyclone seen during September between 23°–24°N is not clear during October and formation anticyclone eddy between 15°-16°N. In the central and southern parts, the flow of the geostrophic currents is towards south along the western coast and towards the north along the eastern side with the presence of cyclonic and anticyclonic eddies in the central axis of the Red Sea with a weak flow. In November and December, the structure of geostrophic currents are similar to that of October but with stronger currents and well established cyclonic and anticyclonic eddies.

During summer, the cyclonic eddies are often concentrated on the west side and the anticyclonic eddies on the eastern side of the Red Sea, while in winter it is the opposite. Their formation might be related to wind forces and thermohaline (Neumann and McGill, 1961; Phillips, 1966; Quadfasel and Baudner, 1993; Siedler, 1969; Tragou and Garrett, 1997).

Since the general circulation in the Red Sea is largely modified with the presence of cyclonic and anticyclonic eddies, the identification of eddies in the study area were conducted based on defining the eddies in terms of SLA (Chelton et al., 2011). Figure 7 shows statistical variability of lifespan, number of eddies, amplitude, and the mean speed of geostrophic current in the center of the eddies with latitude for 6 years. Statistical analysis indicates that eddies are generated over the entire Red Sea, mostly concentrated between 18°-24°N, obviously stronger than any other latitude. The amplitude of an eddy has been defined as the differences between the estimated basic height of the eddy boundary and the extremum value of SLA inside the eddy interior parts. the result indicates the range of amplitude of eddies in the Red Sea is about 4 cm which is an agreement with global values mentioned by (Chelton et al., 2011).

The average lifespan of the cyclonic eddies is longer than that of the anticyclonic eddies. Moreover, the mean speed of geostrophic current for the entire Red Sea is about 5-10 cm/s, which has reached three-times higher in the 25°-26°N latitude band for both cyclonic and anticyclonic. These results match those observed in previous study Zhan et al., (2014).





281 Figure 7. the variability of eddies with latitude for cyclonic (right panel) and anticyclonic (left  
 282 panel).



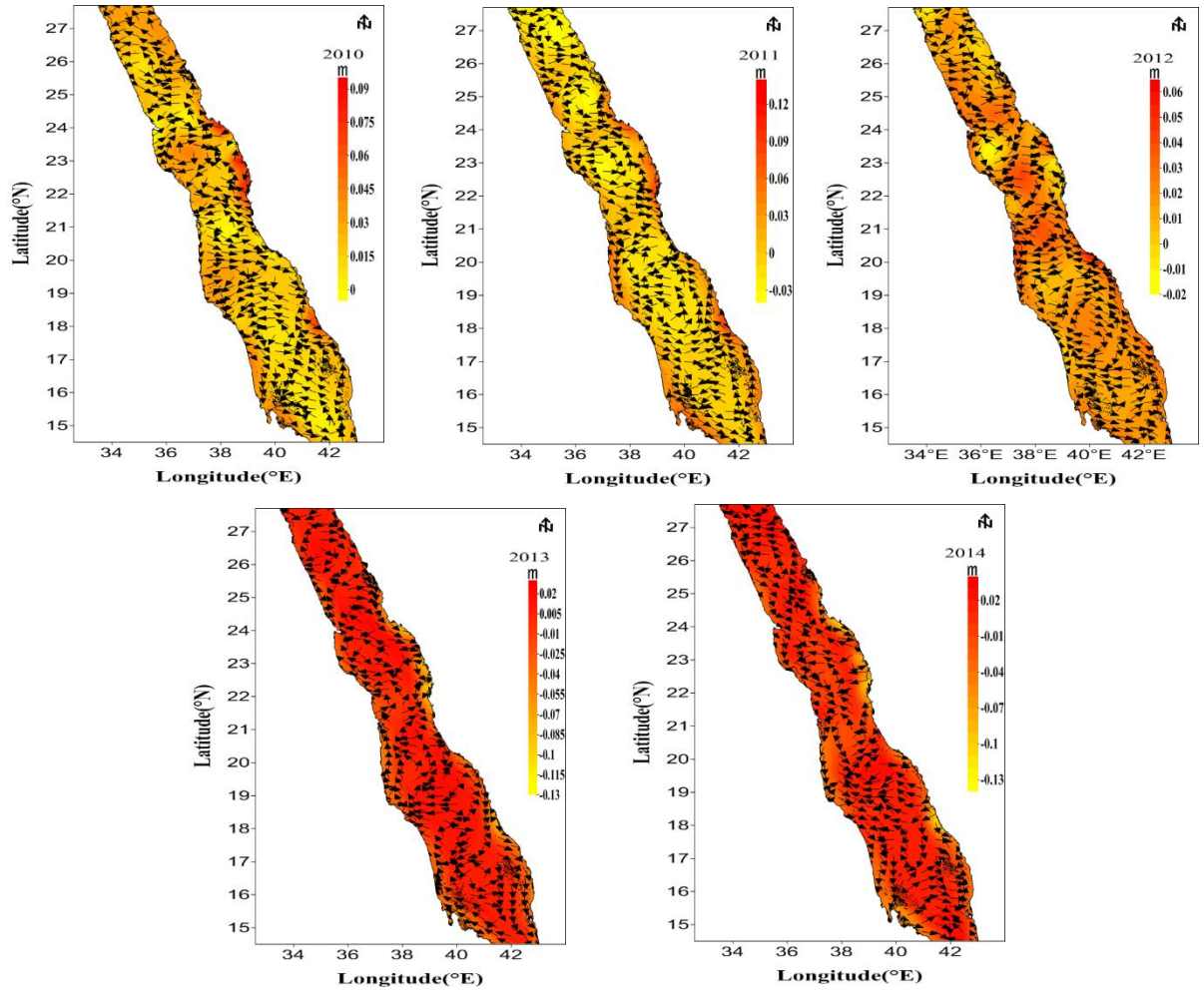


Figure 8. Maps of the annual mean SLA as a deviation from 6-yr mean.

Figure 8 shows the annual mean of SLA as deviation from the 6-year mean. The interannual variability of SLA and geostrophic currents is clearly seen in the southern part of the Red Sea while in the northern part, the pattern is similar for all years except for 2013 where the cyclonic replaced by anticyclonic eddy. The SLA and geostrophic distribution observed during 2011 are similar to that shown in Papadopoulos et al., (2015), with the cyclonic eddy along the eastern side seen more clearly. Moreover, due to extension of our data we could compute the cyclonic pattern up to the coast. The geostrophic currents direction is irregular along the coast, which is northward most of the time. The eddies were mostly concentrated in the north and central parts of the Red Sea.

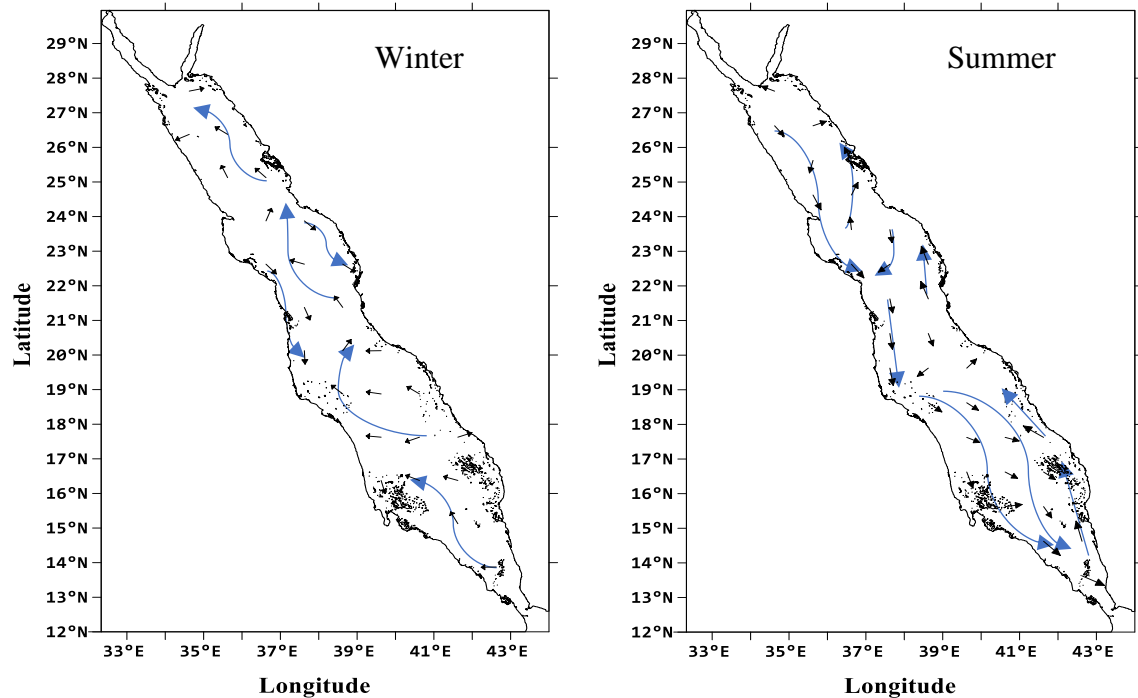


Figure 9. Winter and summer seasonal average surface geostrophic currents, black arrows are actual surface geostrophic currents and blue arrows are schematic streamline.

Figure 9 shows the general schematic of the seasonal variability of geostrophic currents derived from 6 years. During winter, the mean flow is toward the north mostly along the western coast up to 23°N then it shifts to the eastern coast. This result agrees with Sofianos and Johns, (2003). During summer, the flow is towards the south along the western side of the sea while in the southern part the flow spreads for most of the area of the Red Sea with a narrow northward direction near the eastern coast.

303

#### 4. Conclusion

In general, the geostrophic current has been estimated from FSM-SLA for Red Sea region, and the distribution of the geostrophic current shows that the winter period extends from October to May and summer period extends from June to September. This pattern is similar to that shown by (Sofianos and Johns, 2001). There was a lack in measurements of coastal currents in the Red Sea. This study was able to produce data near the coast.

The southern Red Sea show significant interannual variability in the geostrophic current pattern, while the central and northern parts are negligible difference over the years. The geostrophic along the eastern coast is towards the north while along the western coast of the sea it is southward. The mean flow during winter is toward the north mostly along the western coast up to the central Red Sea which shift to the eastern coast in the northern latitudes. This pattern changes by summer to northward flowing eastern coastal current and a southward flowing western coastal current.

The cyclonic eddies were relatively larger than the anticyclonic eddies in the Red Sea. The eddies are concentrated in the central and north of the Red Sea more than in the south. In winter, the cyclonic eddies are beside the west coast and anticyclonic eddies on the east side in the Red Sea, while in summer it is the opposite. Also there is a noticeable change in some eddies from anticyclonic during winter to cyclonic during summer and vice versa in the north between 26.3°N –27.5°N. The analysis of the eddies found that during the summer the cyclonic eddies are dominant than winter in the entire Red Sea, while eddies of both polarities observed during winter. The finding of this paper considered the first of its type in the Red Sea for extending SLA and geostrophic currents to the coast beside giving more details of eddies spatial and temporal variabilities in the coastal region.

## Acknowledgments

The authors are deeply grateful to the data providers. JPL Physical Oceanography Distribution Active Archive Center (PODAAC), the Archiving Validation and Interpretation of Satellite Oceanographic (AVISO) to provide Jason-2 data. This also extends to the Saudi Arabian GCS for providing hourly tide gauge data along the coast of the Red Sea. They are thankful for the High-Performance Computing center at King Abdulaziz University (<http://hpc.kau.edu.sa>) for giving us a chance to use their facilities during analyses of data. Our thanks are for King Abdulaziz University, Jeddah, Saudi Arabia and Hodeidah University, Yemen for making this research possible.

## References

- Abdallah, A. M. and Eid, F. M.: On the steric sea level in the Red Sea, *Int. Hydrogr. Rev.*, 66(1), 115–124., 1989.
- Ahmad, F. and Sultan, S. A. R.: On the heat balance terms in the central region of the Red Sea, *Deep Sea Res. Part A. Oceanogr. Res. Pap.*, 34(10), 1757–1760, 1987.
- Ahmad, F. and Sultan, S. A. R.: Surface heat fluxes and their comparison with the oceanic heat-flow in the red-sea, *Oceanol. acta*, 12(1), 33–36, 1989.
- Al Saafani, M. A. and Shenoi, S. S. C.: Seasonal cycle of hydrography in the Bab el Mandab region, southern Red Sea, *Proc. Indian Acad. Sci. Earth Planet. Sci.*, 113(3), 269–280, doi:10.1007/BF02716725, 2004.
- Andersen, O. B. and Knudsen, P.: The role of satellite altimetry in gravity field modelling in coastal areas, *Phys. Chem. Earth, Part A Solid Earth Geod.*, 25(1), 17–24, doi:10.1016/S1464-1895(00)00004-1, 2000.
- Birol, F., Cancet, M. and Estournel, C.: Aspects of the seasonal variability of the Northern Current ( NW Mediterranean Sea ) observed by altimetry, *J. Mar. Syst.*, 81(4), 297–311, doi:10.1016/j.jmarsys.2010.01.005, 2010.
- Bower, A. and Farrar, J. T.: Air – Sea Interaction and Horizontal Circulation in the Red Sea, in *The Red Sea the Formation, Morphology, Oceanography and Environment of a Young Ocean Basin*, edited by N. M. A. Rasul and I. C. F. Stewart, pp. 329–342, Springer., 2015.
- Chelton, D. B., Schlax, M. G. and Samelson, R. M.: Progress in Oceanography Global observations of nonlinear mesoscale eddies, *Prog. Oceanogr.*, 91(2), 167–216, doi:10.1016/j.pocean.2011.01.002, 2011.
- Chelton, U. B., Ries, J. C., Haines, B. J., FU, L.-L. and Callahan, P. S.: Satellite Altimetry and Earth Sciences, in *Satellite Altimetry and Earth Sciences A Handbook of Techniques and Applications*, edited by L.-L. FU and A. Cazenave, pp. 1–122, Academic Press, San Diego, California ,USA., 2001.
- Chen, C., Li, R., Pratt, L., Limeburner, R., Berdsley, R., Bower, A., Jiang, H., Abualnaja, Y., Xu, Q., Lin, H., Liu, X., Lan, J. and Kim, T.: Process modeling studies of physical mechanisms of the formation of an anticyclonic eddy in the central Red Sea, *J. Geophys. Res. Ocean.*, 119, 1445–1464, doi:10.1002/2013JC009351, 2014.
- Clifford, M., Horton, C., Schmitz, J. and Kantha, L. H.: An oceanographic nowcast/forecast system

for the Red Sea, *J. Geophys. Res. Ocean.*, 102(C11), 25101–25122, doi:10.1029/97JC01919, 1997.

Deng, X. and Featherstone, W. E.: A coastal retracking system for satellite radar altimeter waveforms : Application to ERS-2 around Australia, *J. Geophys. Res.*, 111((C06012)), 1–16, doi:10.1029/2005JC003039, 2006.

Deng, X., Featherstone, W. E., Hwang, C. and Shum, C. K.: Improved Coastal Marine Gravity Anomalies at the Taiwan Strait from Altimeter Waveform Retracking, in *Proceedings of the International Workshop on Satellite Altimetry for Geodesy, Geophysics and Oceanography.*, 2001.

Desportes, C., Obligis, E. and Eymard, L.: On Wet Tropospheric Correction For Altimetry In Coastal Regions, in ‘Envisat Symposium 2007’, Montreux, Switzerland, pp. 23–27., 2007.

Durand, F., Shankar, D., Birol, F. and Shenoi, S. S. C.: Spatio-temporal structure of the East India Coastal Current from satellite altimetry, *J. Geophys. Res. Ocean*, 114(2), 18, doi:10.1029/2008JC004807, 2009.

Edwards, F. J.: *Climate and oceanography, Red sea*, 1, 45–68, 1987.

Eladawy, A., Nadaoka, K., Negm, A., Abdel-Fattah, S., Hanafy, M. and Shaltout, M.: Characterization of the northern Red Sea’s oceanic features with remote sensing data and outputs from a global circulation model, *Oceanologia*, 59(3), 213–237, doi:10.1016/j.oceano.2017.01.002, 2017.

Eshel, G. and Naik, N. H.: Climatological Coastal Jet Collision, Intermediate Water Formation, and the General Circulation of the Red Sea, *Am. Meteorol. Soc.*, (1989), 1233–1257, doi:10.1175/1520-0485, 1997.

Ghosh, S., Kumar Thakur, P., Garg, V., Nandy, S., Aggarwal, S., Saha, S. K., Sharma, R. and Bhattacharyya, S.: SARAL/AltiKa Waveform Analysis to Monitor Inland Water Levels: A Case Study of Maithon Reservoir, Jharkhand, India, *Mar. Geod.*, 38(S1), 597–613, doi:10.1080/01490419.2015.1039680, 2015.

Hwang, C., Guo, J., Deng, X., Hsu, H. Y. and Liu, Y.: Coastal gravity anomalies from retracked Geosat/GM altimetry: Improvement, limitation and the role of airborne gravity data, *J. Geod.*, 80(4), 204–216, doi:10.1007/s00190-006-0052-x, 2006.

Johns, W. E., Jacobs, G. a, Kindle, J. C., Murray, S. P. and Carron, M.: *Arabian Marginal Seas and Gulfs Report of a Workshop held at.*, 2000.

Khaki, M., Forootan, E. and Sharifi, M. A.: Satellite radar altimetry waveform retracking over the

401 Caspian Sea, *Int. J. Remote Sens.*, 35(17), 6329–6356, 2014.

402 Manasrah, R., Badran, M., Lass, H. U. and Fennel, W.: Circulation and winter deep-water  
403 formation in the northern Red Sea, *Oceanologia*, 46(1), 5–23, 2004.

404 Manasrah, R., Hasanean, H. M. and Al-Rousan, S.: Spatial and seasonal variations of sea level in  
405 the Red Sea, 1958-2001, *Ocean Sci. J.*, 44(3), 145–159, doi:10.1007/s12601-009-0013-4, 2009.

406 Mantripp, D.: Radar altimetry, in *The Determination of Geophysical Parameters From Space*,  
407 edited by N. . Fancey, I. . Gardiner, and R. A. Vaughan, p. 119, Institute of Physics Publishing,  
408 London, UK., 1966.

409 Morcos, S. A.: Physical and chemical oceanography of the Red Sea, *Ocean. Mar. Biol. Ann. Rev.*,  
410 8, 73–202, 1970.

411 Murray, S. P. and Johns, W.: Direct observations of seasonal exchange through the Bab el Mandab  
412 Strait, *Geophys. Res. Lett.*, 24(21), 2557–2560, 1997.

413 Neumann, A. C. and McGill, D. A.: Circulation of the Red Sea in early summer, *Deep Sea Res.*,  
414 8(3–4), 223–235, 1961.

415 Osman, M.: Evaporation from coastal water off Port-Sudan, *J. King Abdulaziz Univ. Mar. Sci.*,  
416 17(4), 1–2, 1985.

417 Papadopoulos, V. P., Zhan, P., Sofianos, S. S., Raitsos, D. E., Qurban, M., Abualnaja, Y., Bower,  
418 A., Kontoyiannis, H., Pavlidou, A. and Asharaf, T. T. M.: Factors governing the deep ventilation  
419 of the Red Sea, *J. Geophys. Res. Ocean.*, 120(11), 7493–7505, 2015.

420 Patzert, W. C.: Wind-induced reversal in Red Sea circulation, *Deep Sea Res. Oceanogr.*, 21(2),  
421 109–121, 1974.

422 Phillips, O. M.: On turbulent convection currents and the circulation of the Red Sea, *Deep Sea*  
423 *Res.*, 13(6), 1149–1160, 1966.

424 Quadfasel, D. and Baudner, H.: Gyre-scale circulation cells in the Red-Sea, *Oceanol. Acta*, 16(3),  
425 221–229, 1993.

426 Schmidt, M., Devey, C. and Eisenhauer, A.: FS Poseidon Fahrtbericht/Cruise Report P408  
427 [POS408]-The Jeddah Transect; Jeddah-Jeddah, Saudi Arabia, 13.01.-02.03. 2011.

428 Siedler, G.: General circulation of water masses in the Red Sea, in *Hot Brines and Recent Heavy*  
429 *Metal Deposits in the Red Sea*, edited by E. T. DEGENS and D. A. Ross, pp. 131–137, Springer-  
430 Verlag, New York., 1969.

431 Smeed, D. A.: Exchange through the Bab el Mandab, *Deep Sea Res. Part II Top. Stud. Oceanogr.*,

51(4), 455–474, 2004.

Sofianos, S. and Johns, W. E.: Water mass formation, overturning circulation, and the exchange of the Red Sea with the adjacent basins, in *The Red Sea the Formation, Morphology, Oceanography and Environment of a Young Ocean Basin*, edited by N. M. A. Rasul and I. C. F. Stewart, pp. 343–353, Springer., 2015.

Sofianos, S. S.: An Oceanic General Circulation Model (OGCM) investigation of the Red Sea circulation: 2. Three-dimensional circulation in the Red Sea, *J. Geophys. Res.*, 108(C3), 3066, doi:10.1029/2001JC001185, 2003.

Sofianos, S. S. and Johns, W. E.: An Oceanic General Circulation Model (OGCM) investigation of the Red Sea circulation, 1. Exchange between the Red Sea and the Indian Ocean, *J. Geophys. Res.*, 107(C11), 3196, doi:10.1029/2001JC001184, 2002.

Sofianos, S. S. and Johns, W. E.: Observations of the summer Red Sea circulation, *J. Geophys. Res.*, 112, 1–20, doi:10.1029/2006JC003886, 2007.

Sofianos, S. S. and Johns, W. E.: Wind induced sea level variability in the Red Sea, *Geophys. Res. Lett.*, 28(16), 3175–3178, 2001.

Sultan, S. A. R. and Elghribi, N. M.: Sea level changes in the central part of the Red Sea, *Indian J. Mar. Sci.*, 32(2), 114–122, 2003.

Sultan, S. A. R., Ahmad, F. and Nassar, D.: Relative contribution of external sources of mean sea-level variations at Port Sudan, Red Sea, *Estuar. Coast. Shelf Sci.*, 42(1), 19–30, 1996.

Taqi, A. M., Al-Subhi, A. M. and Alsaafani, M. A.: Extension of Satellite Altimetry Jason-2 Sea Level Anomalies Towards the Red Sea Coast Using Polynomial Harmonic Techniques, *Mar. Geod.*, doi:10.1080/01490419.2017.1333549, 2017.

Tragou, E. and Garrett, C.: The shallow thermohaline circulation of the Red Sea, *Deep Sea Res. Part I Oceanogr. Res. Pap.*, 44(8), 1355–1376, 1997.

Vignudelli, S., Cipollini, P., Astraldi, M., Gasparini, G. P. and Manzella, G.: Integrated use of altimeter and in situ data for understanding the water exchanges between the Tyrrhenian and Ligurian Seas, *J. Geophys. Res.*, 105(C8), 19649–19664, doi:doi:10.1029/2000JC900083, 2000.

Vignudelli, S., Cipollini, P., Roblou, L., Lyard, F., Gasparini, G. P., Manzella, G. and Astraldi, M.: Improved satellite altimetry in coastal systems: Case study of the Corsica Channel (Mediterranean Sea), *Geophys. Res. Lett.*, 32(L07608), 1–5, doi:10.1029/2005GL022602, 2005.

Yao, F., Hoteit, I., Pratt, L. J., Bower, A. S., Zhai, P., Kohl, A. and Gopalakrishnan, G.: Seasonal

463 overturning circulation in the Red Sea: 1. Model validation and summer circulation, J. Geophys.  
464 Res. Ocean., 119, 2238–2262, doi:10.1002/2013JC009331.Key, 2014a.  
465 Yao, F., Hoteit, I., Pratt, L. J., Bower, A. S., Köhl, A., Gopalakrishnan, G. and Rivas, D.: Seasonal  
466 overturning circulation in the Red Sea: 2. Winter circulation, J. Geophys. Res. Ocean., 119(4),  
467 2263–2289, doi:10.1002/2013JC009331, 2014b.  
468 Zhan, P., Subramanian, A. C., Yao, F. and Hoteit, I.: Eddies in the Red Sea: A statistical and  
469 dynamical study. Geophys. Res. Ocean., 119, 3909–3925, doi:10.1002/2013JC009563, 2014.  
470  
471